SARS-CoV-2 B.1.617.2 Delta variant emergence and vaccine breakthrough

Petra Mlcochova[1,2]*, Steven Kemp[1,2]*, Mahesh Shanker Dhar[3]*, Guido Papa[4], Bo Meng[1,2], Swapnil Mishra[5], Charlie Whittaker[5], Thomas Mellan[5], Isabella Ferreira[1,2], Rawlings Datir[1,2], Dami A. Collier[2,6], Sujeet Singh[3], Rajesh Pandey[7], Robin Marwal[3], Meena Datta[3], Shantanu Sengupta[7], Kalaiarasan Ponnusamy[3], V.S. Radhakrishnan[3], Adam Abdullahi[1,2], Niluka Goonawardne[8], Jonathan Brown[8], Oscar Charles[6], Partha Chattopadhyay[7], Priti Devi[7], Daniela Caputo[9], Tom Peacock[8], Dr Chand Wattal[10], Neeraj Goel[10], Raju Vaishya[11], Meenakshi Agarwal[12], The Indian SARS-CoV-2 Genomics Consortium (INSACOG), The CITIID-NIHR BioResource COVID-19 Collaboration, Antranik Mavousian[13], Joo Hyeon Lee[13,14], Wendy S. Barclay[8], Samir Bhatt[4,15], Seth Flaxman[16], Leo James[4], Partha Rakshit[3*], Anurag Agrawal[7*], Ravindra K. Gupta[1,2, 17*]

[1] Cambridge Institute of Therapeutic Immunology & Infectious Disease (CITIID), Cambridge, UK.

[2] Department of Medicine, University of Cambridge, Cambridge, UK.

[3] National Centre for Disease Control, Delhi, India

[4] MRC – Laboratory of Molecular Biology, Cambridge, UK.

[5] Medical Research Council (MRC) Centre for Global Infectious Disease Analysis, Jameel Institute, School of Public Health, Imperial College London, UK.

[6] University College London, London, UK

[7] CSIR Institute of Genomics and Integrative Biology, Delhi, India

[8]Department of Infectious Diseases, Imperial College London, UK.

[9] NIHR Bioresource, Cambridge, UK

[10] Sri Ganga Ram Hospital, New Delhi, India

[11] Indraprastha Apollo Hospital, New Delhi

[12] Northern Railway Central Hospital, New Delhi, India

[13] Wellcome-MRC Cambridge Stem Cell Institute, Cambridge, UK.

[14]Department of Physiology, Development and Neuroscience, University of Cambridge, Cambridge, UK.

[15] Section of Epidemiology, Department of Public Health, University of Copenhagen, Denmark

[16] Department of Mathematics, Imperial College London, London, UK

[17]Africa Health Research Institute, Durban, South Africa.

*Authors contributed equally to this work

Address for correspondence:

rkg20@cam.ac.uk; a.agrawal@igib.in; partho_rakshit@yahoo.com

Key words: SARS-CoV-2; COVID-19; B.1.617; antibody escape; neutralising antibodies; infectivity; spike mutation; evasion; resistance; fitness; Delta variant

Abstract

The SARS-CoV-2 B.1.617.2 (Delta) variant was first identified in the state of Maharashtra in late 2020 and has spread throughout India, displacing the B.1.1.7 (Alpha) variant and other pre-existing lineages. Mathematical modelling indicates that the growth advantage is most likely explained by a combination of increased transmissibility and immune evasion. Indeed *in vitro*, the delta variant is less sensitive to neutralising antibodies in sera from recovered individuals, with higher replication efficiency as compared to the Alpha variant. In an analysis of vaccine breakthrough in over 100 healthcare workers across three centres in India, the Delta variant was responsible for greater transmission between HCW as compared to B.1.1.7 or B.1.617.1 (mean cluster size 3.2 versus 1.1, p<0.05). *In vitro*, the Delta variant shows 8 fold approximately reduced sensitivity to vaccine-elicited antibodies compared to wild type Wuhan-1 bearing D614G. Serum neutralising titres against the SARS-CoV-2 Delta variant were significantly lower in participants vaccinated with ChadOx-1 as compared to BNT162b2 (GMT 3372 versus 654, p<0001). These combined epidemiological and *in vitro* data indicate that the dominance of the Delta variant in India has been most likely driven by a combination of evasion of neutralising antibodies in previously infected individuals and increased virus infectivity. Whilst severe disease in fully vaccinated HCW was rare, breakthrough transmission clusters in hospitals associated with the Delta variant are concerning and indicate that infection control measures need continue in the post-vaccination era.

Introduction

Although vaccines have been available since early 2021, achieving near universal coverage has in adults has been an immense logistical challenge, in particular for populous nations. India's first wave of SARS-CoV-2 infections in mid 2020 was relatively mild and was controlled by a nationwide lockdown. Since easing of restrictions, India has seen expansion in cases of COVID-19 since March 2021 with widespread fatalities and a death toll of over 300,000. The B.1.1.7 variant, introduced by travel from the UK in late 2020, grew in the north of India and is known to be more transmissible than previous viruses bearing the D614G spike mutation, whilst maintaining sensitivity to vaccine elicited neutralising antibodies[1,2]. The B.1.617 variant emerged in the state of Maharashtra in late 2020/early 2021[3] , spreading throughout India and to at least 60 countries. The first sublineage to be detected was B.1.617.1, followed by B.1.617.2, both bearing the L452R spike mutation also observed in the 'California Variant' B.1.429.

Here we analyse the growth and dominance of the B.1.617.2 Delta variant in Mumbai, with modelling indicating that combined effects of viral transmissibility and immune evasion are responsible. We find the Delta variant exhibits higher replication in airway cells and its spike protein mediates more efficient cell entry and augmented syncytium formation. We also find significantly reduced sensitivity of B.1.617.2 to convalescent sera and vaccine-elicited antibodies, manifesting in Indian vaccinated healthcare workers (HCW) as symptomatic breakthrough infection, dominated by B.1.617.2 and leading to significant transmission chains.

Results

B.1.617.2 Delta variant growth advantage due to re-infection and increased transmissibility

We plotted the relative proportion of variants in new cases of SARS-CoV-2 in India since the start of 2021. Whilst B.1.617.1 emerged earlier, it has been replaced by the Delta variant B.1.617.2 (**Figure 1a**). Next, we attempted to characterise the Delta variant's epidemiological properties in further detail through dynamical modelling of the recent resurgence of SARS-CoV-2 transmission in Mumbai. We utilise a Bayesian model of SARS-CoV-2 transmission and mortality that simultaneously models two categories of virus

("delta" and "non-delta") and that allows the epidemiological properties (such as transmissibility and capacity to reinfect previously infected individuals) to vary between categories[4]. This model also explicitly incorporates waning of immune protection following infection, parameterised using the results of recent longitudinal cohort studies (api.covid19india.org). The model integrates epidemiological data on daily COVID-19 mortality, serological data from the city spanning July - December 2020[5] and genomic sequence data from GISAID (with lineage classification carried out using the Pangolin software tool (https://pangolin.cog-uk.io/)[6], (**Figure 1b,c).** There are substantial uncertainties in the date of the Delta variant's introduction into Mumbai, as well as the degree of COVID-19 death under- ascertainment in Mumbai to date. We therefore explore a range of different scenarios varying underreporting (30% and 50%) and introduction dates (31st Jan 2021, 1st Jan 2021 and 1st Dec 2020). Full results for the different scenarios are present in the **Extended Data Table 1**. Across all scenarios considered, our results suggest the Delta variant as both more transmissible and better able to evade prior immunity elicited by previous infection compared to previously circulating lineages. Results for the scenario assuming 50% death underreporting and an introduction date of 31st Jan 2021 are presented (**Figure 1d**). For these we estimate that the Delta variant is 1.1- to 1.4-fold (50% bCI) more transmissible than previously circulating lineages in Mumbai, and that B.1.617.2 is able to evade 20 to 55% of the immune protection provided by prior infection with non-B.1.617.2 lineages.

Delta variant is less sensitive to neutralising antibodies from recovered individuals.

We next sought biological support for the inferences from mathematical modelling. We used sera from twelve individuals infected during the first UK wave in mid-2020 (likely following infection with SARS-CoV-2 Wuhan-1). These sera were tested for ability to neutralise a Delta variant viral isolate (**Figure 1e**) obtained from nose/throat swab, in comparison to an Alpha B.1.1.7 variant isolate and a wild type (WT) Wuhan-1 virus bearing D614G in spike. The Delta variant contains several spike mutations that are located at positions within the structure that are predicted to alter its function (**Figure 1e**). We found that the Alpha variant was 2.3-fold less sensitive to the sera compared to the WT, and that the Delta variant virus was 5.7-fold less sensitive to the sera (**Figure 1f**). Importantly in the same assay, the Beta variant (B.1.351) that emerged in South Africa demonstrated an 8.2 fold loss of neutralisation sensitivity relative to WT.

Delta variant shows higher replication in human primary airway cells

We next sought biological evidence for the higher transmissibility predicted from the modelling. Increased replication could be responsible for generating greater numbers of virus particles, or the particles themselves could be more likely to lead to a productive infection. We infected primary 3D airway organoids[7] (**Figure 2a**) with the Delta variant and compared intracellular viral RNA quantities with those generated during infection with the Alpha variant over 48 hours. In addition we measured cell free virus produced from organoids by infecting target Vero cells with culture media from the airway cells. We noted a significant replication advantage for Delta over Alpha, with almost one log greater N gene copy number in cells after 24 hours (**Figure 2b**).

B.1.617.2 spike has enhanced entry efficiency associated with cleaved spike

Spike is known to mediate cell entry via interaction with ACE2 and TMPRSS2[8] and is a major determinant of viral infectivity. In order to gain insight into the mechanism of increased infectivity of Delta, we tested single round viral entry of B.1.617.1 and B.1.617.2 spikes (**Figure 2c**) using the PV system, infecting primary 3D airway organoids and Calu-3 lung cells expressing endogenous levels of ACE2 and TMPRSS2, as well as other cell lines transduced or transiently transfected with ACE2 / TMPRSS2 (**Figure 2d, e**). We first probed PV virions and cell lysates for spike protein and noted that the B.1.617 spikes were present predominantly in cleaved form in cells and virions, in contrast to WT (**Figure 2d**). We observed one log increased entry efficiency for both B.1.617.1 and B.1.617.2. over Wuhan-1 D614G wild type in nearly all cells tested (**Figure 2e**). SARS-CoV-2 infection in clinically relevant cells is TMPRSS2 dependent and requires fusion at the plasma membrane, potentially to avoid restriction factors in endosomes[9]. We found that B.1.617.2 was marginally less sensitive to the TMPRSS2 inhibitor Camostat (**Figure 2f**). Addition of the cathepsin inhibitor, which blocks endosomal viral entry, had no impact as predicted.

Transmission clusters in vaccinated health care workers associated with Delta variant

Having gathered epidemiological and biological evidence that the Delta variant's growth advantage over other lineages might relate to increased transmissibility as well as re-infection in a population with low vaccine coverage (<20% with a single dose), we hypothesised that vaccine efficacy could be compromised by the Delta Variant.

Although overall national vaccination rates were low in India in the first quarter of 2021, vaccination of health care workers (HCW) started in early 2021 with the ChadOx-1 vaccine (Covishield). During the wave of infections during March and April an outbreak of symptomatic SARS-CoV-2 was confirmed in 30 vaccinated staff members amongst an overall workforce of 3800 at a single tertiary centre in Delhi by RT-PCR of nasopharyngeal swabs (age range 27-77 years). Genomic data from India suggested B.1.1.7 dominance overall (Figure 1a) and in the Delhi area during the first quarter of 2021 (**Figure 3a**), with growth of B.1.617 during March 2021. 385 out of 604 sequences reported to GISAID in April 2021 for Delhi were B.1.617.2. Short-read sequencing[10] of symptomatic individuals in the HCW outbreak revealed the majority were B.1.617.2 with a range of other B lineage viruses including B.1.1.7 (**Figure 3b**). There were no cases that required ventilation though one HCW received oxygen therapy. Further analysis of pairwise differences demonstrated a group of highly related, and in some cases, genetically indistinct sequences (**Figure 3c**). Maximum likelihood phylogenetic analysis of consensus sequences from symptomatic HCW breakthrough infections revealed that eleven B.1.617.2 viruses were almost identical and were sampled within one or two days of each other. These data are consistent with a single transmission from an infected individual (**Figure 3c**). To contextualise the outbreak sequences, a further phylogeny was inferred with a random subsample of Indian B.1.617 sequences downloaded from GISAID and the outbreak sequences added (**Extended Data Figure 1**), demonstrating clonal sequences that clustered within locally sequenced isolates. We next looked in greater detail at the vaccination history of cases. Nearly all had received two doses at least 21 days previously, and median time since second dose was 27 days (**Figure 3c**).

We obtained similar data on breakthrough infections and ChadOx-1 vaccination status in two other health facilities in Delhi with 1100 and 4000 HCW staff members respectively (Figure 2D). In hospital two there were 51 such sequences from 70 symptomatic infections for which reconstructed phylogenies from 57 with high quality whole genome coverage; in hospital three there were 118 symptomatic infections documented, with 57 used for reconstruction of phylogenies (**Figure 3d,e, Extended Data Table 2**). As expected, we observed that the Delta variant dominated vaccine-breakthrough infections in both centres, demonstrating significant respiratory viral load with median Ct values below 20 (**Extended Data Figure 1**). We proceeded to analyse instances of onward transmissions within HCW, and we defined related or ‘linked’ infections as differing by six nucleotides or less. Importantly, in this vaccinated

population across three hospitals, the Delta variant was associated with greater transmissions to other HCW as compared to B.1.1.7 or B.1.617.1 (mean cluster size 3.2 versus 1.1, p<0.05, **Extended Data Figure 1**). This association between Delta and cluster size persisted when we performed regression analysis incorporating hospital into the model as a variable. There were no clusters of non-Delta infections comprising >2 individuals, whereas there were ten such clusters for Delta variant (**Extended Data Figure 1**). The vaccine responses of HCW with subsequent breakthrough were measured and appeared similar to responses in a control group of HCW that did not test positive for SARS-CoV-2 subsequently (**Extended Data Figure 1**).

B.1.617.2 Delta Variant is less sensitive to vaccine-elicited antibodies than Alpha Variant

We used a Delta variant live virus isolate to test susceptibility to vaccine elicited neutralising antibodies in individuals vaccinated with ChAdOx-1 or BNT162b2. These experiments showed a loss of sensitivity for B.1.617.2 compared to wild type Wuhan-1 bearing D614G of around 8-fold for both sets of vaccine sera and reduction against B.1.1.7 that did not reach statistical significance (**Figure 4a**). We also used a PV system to test neutralisation potency of a larger panel of 65 vaccine-elicited sera (**Extended Data Table 3**), this time against B.1.617.1 as well as B.1.617.2 spike compared to Wuhan-1 D614G spike (**Figure 4b**). Comparison of demographic data for each individual showed similar characteristics (**Extended Data Table 3**). The mean GMT against Delta Variant spike PV was lower for ChAdOx-1 compared to BNT162b2 (GMT 3372 versus 654, p<0001, **Extended Data Table 3)**. We observed a fold change loss of neutralisation against B.1.617.2 of 6.2 for ChAdOx-1 and 2.9 for BNT162b2 (**Figure 4b**). GMT for B.1.617.2 and B.1.617.1 were similar to one another (**Figure 4b**).

B.1.617.2 spike confers increased syncytium formation

The plasma membrane route of entry, and indeed transmissibility in animal models, is critically dependent on the polybasic cleavage site (PBCS) between S1 and S2[9,11,12]and cleavage of spike prior to virion release from producer cells; this contrasts with the endosomal entry route, which does not require spike cleavage in producer cells. [9,13,14]. Mutations at P681 in the PBCS have been observed in multiple SARS-CoV-2 lineages, most notably in the B.1.1.7 Alpha variant[15]. We previously showed that B.1.1.7 spike, bearing P681H, had significantly higher fusogenic potential than a D614G Wuhan-1 virus[13]. We next tested B.1.617.1 and B.1.617.2 spike using a split GFP system to monitor cell-cell fusion

(**Extended Data Figure 2a, b, c**). We transfected spike bearing plasmids into Vero cells stably expressing the two different part of Split-GFP, so that GFP signal could be measure over time upon cell-cell fusion (**Extended Data Figure 2d**). The B.617.1 and B.617.2 spikes demonstrated higher fusion activity and syncytium formation, mediated specifically by P681R (**Extended Data Figure 2d,e**). We next tested the ability of CMK to inhibit cell-cell fusion, a process that requires cleaved spike. CMK is a furin inhibitor and normally blocks cell-cell fusion[16-18]. We found that fusion mediated by the Delta variant spike was marginally less sensitive to CMK relative to WT (**Extended Data Figure 2f**), possibly due to greater inherent S1/S2 cleavage (**Extended Data Figure 2c**). Finally we explored whether post vaccine sera could block syncytia formation, as this might be a mechanism for vaccine protection against pathogenesis. We titrated sera from ChAdOx-1 vaccinees and showed that indeed the cell-cell fusion could be inhibited in a manner that mirrored neutralisation activity of the sera against PV infection of cells (**Extended Data Figure 2g**). Hence the Delta variant may induce cell-cell fusion in the respiratory tract and possibly higher pathogenicity even in vaccinated individuals with neutralising antibodies.

Discussion

Here we have combined modelling, molecular epidemiology and *in vitro* experimentation to propose that increased replication fitness and reduced sensitivity of B.1.617.2 Delta Variant to neutralising antibodies from past infection contributed to the devastating epidemic wave in India during the first quarter of 2021, where background infection to the Wuhan-1 D614G in 2020 was between 20-50%[19] and vaccination with at least one dose below 20%.

The modelling results relate to a population for which the vast majority of immunity has arisen from prior infection rather than vaccination. Previous work has shown differences in the breadth and quality of immunity elicited by natural infection compared to immunity[6], and so the degree to which these results generalise to vaccine-derived immunity is likely limited. In addition, GISAID is not representative. Therefore, we made the simplifying assumption that Maharashtra genomic data reflects Mumbai. Furthermore, the inferred transmission advantage is some function of the underlying genetic background Delta emerged in (e.g. B.1.1.7 and B.1.617.1 also present) - therefore this result likely does not generalise to backgrounds e.g. lacking a starting baseline of B.1.1.7 and B.1.617.1. In absence of this baseline (i.e. of other likely highly transmissible VOCs), inferred transmission advantage would probably be even greater. Finally, there was uncertainty in death reporting and start

date remain significant and relevant factors to consider and quantitatively (though not qualitatively) alter the presented results.

Consistent with immune evasion by the Delta Variant, we also show significant numbers of vaccine breakthrough infections in health care workers at three Delhi hospitals, most of whom were fully vaccinated. These infections were predominantly B.1.617.2 Delta Variant, with a mix of other lineages bearing D614G in spike, reflecting prevalence in community infections. Importantly, however, we noted evidence for larger transmission clusters for Delta versus non-Delta infections in these HCW. These observations parallel the higher secondary attack rate in non-household contacts recently reported in the UK of 7% (6.4-7.5%) for Delta vs 4.5% (4.2-4.8%). for Alpha (PHE Variant Technical Briefing 16). Furthermore, transmissions in vaccinated HCW may involve significant proportion of infections due to overdispersion or 'super-spreading'[20], and indeed we document such an event in one of three hospitals studied.

We demonstrate evasion of neutralising antibodies by the Delta variant live virus with sera from convalescent patients, as well as sera from individuals in the UK vaccinated with two different vaccines, one based on an adenovirus vector (ChAdOx-1), and the other mRNA (BNT162b2). Our findings on reduced susceptibility of Delta to vaccine elicited sera are similar to other reports[21,22], including the lower GMT following two doses of ChAdOx-1 compared to BNT162b2. The vaccine sera data presented are consistent with emerging data from observational studies on vaccine efficacy (VE) in the UK, showing that VE is lower for the Delta versus the Alpha variant following both first and second doses of vaccine (PHE Technical Briefing 16). Although we did not map the mutations responsible, previous work with shows that L452R and T478K in the RBD are likely to have contributed[23], as well as NTD mutations such as T19R.

Our work also shows that that the Delta variant virus had a fitness advantage compared to the Alpha variant in a validated 3D respiratory organoid system[7]. We also measured spike mediated entry into target cells exogenously or endogenously expressing ACE2 and TMPRSS2 receptors using a PV system. We observed that the Delta variant had increased entry efficiency relative to wild type Wuhan D614G spike in the respiratory organoids as well as other cells. The Delta variant also appeared more efficient in entry than the related B1.1.617.1, potentially explaining the greater success of the Delta variant. The increased

entry efficiency was associated with higher levels of cleaved spike observed for the Delta variant, likely facilitated by P681R near the PBCS. Interestingly the Delta variant spike PV appeared less sensitive to pharmacological TMPRSS2 inhibition than either WT Wuhan-1 D614G or B.1.617.1, consistent with higher levels of cleaved spike in Delta spike PV.

Virus infectivity and fusogenicity mediated by the PBCS is a key determinant of pathogenicity and transmissibility[9,24] and there are indications that giant cells/syncitia formation are associated with fatal disease[25]. Spike cleavage and stability of cleaved spike are likely therefore to be critical parameters for future SARS-CoV-2 variants of concern.

The B.1.617.2 Delta variant appears more transmissible than B.1.1.7 in the UK based on recent data and the dominance of new infections by this variant. In the absence of published data on transmissibility of the Delta variant we predict that this variant will have a transmission advantage relative to Wuhan-1 with D614G in individuals with pre-existing immunity from vaccines/natural infection as well as in settings where there is low vaccine coverage and low prior exposure. Lower protection against B.1.351, the variant with least sensitivity to neutralising antibodies, has been demonstrated for at least three vaccines[26-29]. However, progression to severe disease and death was low in all studies. Therefore, at population scale, extensive vaccination will likely protect against moderate to severe disease and will reduce transmission of the Delta variant.

However, vaccine breakthrough clusters amongst HCW is of concern given that hospitals frequently treat individuals who may have suboptimal immune responses to vaccination due to comorbidity. Such patients could be at risk for severe disease following infection from HCW or other staff within hospital environments. Therefore strategies to boost vaccine responses against variants are warranted in HCW and attention to infection control procedures should be continued even in the post vaccine era.

Methods

Sequencing Quality Control and Phylogenetic Analysis

Three sets of fasta concensus sequences were kindly provided by three separate Hospitals in Delhi, India. In total, Hospital One consisted of 38 sequences, Hospital Two of 119 sequences, and Hospital Three of 71 sequences. Initially, all sequences were concatenated into a multi-fasta, according to hospital, and then aligned to reference strain MN908947.3 (Wuhan-Hu-1) with mafft v4.475 [30] using the --keeplength --addfragments options. Following this, all sequences were passed through Nextclade v0.14.4 (https://clades.nextstrain.org/) to determine the number of gap regions. This was noted and all sequences were assigned a lineage with Pangolin v3.0.5[6] and pangoLEARN (dated 10th Jun 2021). Sequences that could not be assigned a lineage were discarded. After assigning lineages, all sequences with more than 5% N-regions) were also excluded. After excluding poor-quality sequences, 28 remained for Hospital One, 63 for Hospital Two, and 51 for Hospital Three.

Phylogenies were inferred using maximum-likelihood in IQTREE v2.1.4[31] using a GTR+R6 model and the -fast option. The inferred phylogenies were annotated in R v4.1.0 using ggtree v3.0.2[32] and rooted on the SARS-CoV-2 reference sequence (MN908947.3), and nodes arranged in descending order. Major lineages were annotated on the phylogeny as coloured tips, and a heatmap defining the number of COVIVAX vaccinates received from each patient was added. Finally, where available, cycle threshold (Ct) values were also added to each branch tip on each figure, where available.

Area plots and metadata

Area plots were constructed in RStudio v4.1.0 using the ggplot2 package v3.3.3. Data to populate the plot was downloaded from the GISAID[33] (http://gisaid.org) database. Sequence metadata for the entire database was downloaded on 8th June 2021 and filtered by location

(United Kingdom, or Asia / India). The number of assigned lineages was counted for each location and the most prevalent 15 lineages were retained for plotting.

Structural Analyses

The PyMOL Molecular Graphics System v.2.4.0 (https://github.com/schrodinger/pymol-open-source/releases) was used to map the location of the mutations defining the Delta lineage (B.1.617.2) onto closed-conformation spike protein - PDB: 6ZGE[34].

Serum samples and ethical approval

Ethical approval for use of serum samples. Controls with COVID-19 were enrolled to the NIHR BioResource Centre Cambridge under ethics review board (17/EE/0025).

Cells

HEK 293T CRL-3216, Hela-ACE-2 (Gift from James Voss), Vero CCL-81 were maintained in Dulbecco's Modified Eagle Medium (DMEM) supplemented with 10% fetal calf serum (FCS), 100 U/ml penicillin, and 100mg/ml streptomycin. All cells were regularly tested and are mycoplasma free. H1299 cells were a kind gift from Sam Cook. Calu-3 cells were a kind gift from Paul Lehner, A549 A2T2 (Rihn et al., 2021) cells were a kind gift from Massimo Palmerini. Vero E6 Ace2/TMPRSS2 cells were a kind gift from Emma Thomson.

Pseudotype virus preparation

Plasmids encoding the spike protein of SARS-CoV-2 D614 with a C terminal 19 amino acid deletion with D614G were used. Mutations were introduced using Quickchange Lightning Site-Directed Mutagenesis kit (Agilent) following the manufacturer's instructions. B.1.1.7 S expressing plasmid preparation was described previously, but in brief was generated by step wise mutagenesis. Viral vectors were prepared by transfection of 293T cells by using Fugene HD transfection reagent (Promega). 293T cells were transfected with a mixture of 11ul of Fugene HD, 1µg of pCDNAΔ19 spike-HA, 1ug of p8.91 HIV-1 gag-pol expression vector and 1.5µg of pCSFLW (expressing the firefly luciferase reporter gene with the HIV-1 packaging signal). Viral supernatant was collected at 48 and 72h after transfection, filtered through 0.45um filter and stored at -80˚C as previously described. Infectivity was measured by luciferase detection in target 293T cells transfected with TMPRSS2 and ACE2.

Standardisation of virus input by SYBR Green-based product-enhanced PCR assay (SG-PERT)

The reverse transcriptase activity of virus preparations was determined by qPCR using a SYBR Green-based product-enhanced PCR assay (SG-PERT) as previously described[35]. Briefly, 10-fold dilutions of virus supernatant were lysed in a 1:1 ratio in a 2x lysis solution (made up of 40% glycerol v/v 0.25% Triton X-100 v/v 100mM KCl, RNase inhibitor 0.8 U/ml, TrisHCL 100mM, buffered to pH7.4) for 10 minutes at room temperature.

12µl of each sample lysate was added to thirteen 13µl of a SYBR Green master mix (containing 0.5µM of MS2-RNA Fwd and Rev primers, 3.5pmol/ml of MS2-RNA, and 0.125U/µl of Ribolock RNAse inhibitor and cycled in a QuantStudio. Relative amounts of reverse transcriptase activity were determined as the rate of transcription of bacteriophage MS2 RNA, with absolute RT activity calculated by comparing the relative amounts of RT to an RT standard of known activity.

Plasmids for split GFP system to measure cell-cell fusion

pQCXIP□BSR□GFP11 and pQCXIP□GFP1□10 were from Yutaka Hata [36] Addgene plasmid #68716; http://n2t.net/addgene:68716; RRID:Addgene_68716 and Addgene plasmid #68715; http://n2t.net/addgene:68715; RRID:Addgene_68715)

Generation of GFP1□10 or GFP11 lentiviral particles

Lentiviral particles were generated by co-transfection of Vero cells with pQCXIP□BSR□GFP11 or pQCXIP□GFP1□10 as previously described [37]. Supernatant containing virus particles was harvested after 48 and 72 hours, 0.45 µm filtered, and used to infect 293T or Vero cells to generate stable cell lines. 293T and Vero cells were transduced to stably express GFP1□10 or GFP11 respectively and were selected with 2 µg/ml puromycin.

Cell-cell fusion assay

Cell-cell fusion assay was carried out as previously described [37,38] but using a Split-GFP system. Briefly, Vero GFP1-10 and Vero-GFP11 cells were seeded at 80% confluence in a 1:1 ration in 24 multiwell plate the day before. Cells. were co-transfected with 0.5 µg of spike expression plasmids in pCDNA3 using Fugene 6 and following the manufacturer's instructions (Promega). Cell-cell fusion was measured using an Incucyte and determined as the proportion of green area to total phase area. Data were then analysed using Incucyte

software analysis. Graphs were generated using Prism 8 software. Furin inhibitor CMK (Calbiochem) was added at transfection.

Western blotting

Cells were lysed and supernatants collected 18 hours post transfection. Purified virions were prepared by harvesting supernatants and passing through a 0.45 µm filter. Clarified supernatants were then loaded onto a thin layer of 8.4% optiprep density gradient medium (Sigma-Aldrich) and placed in a TLA55 rotor (Beckman Coulter) for ultracentrifugation for 2 hours at 20,000 rpm. The pellet was then resuspended for western blotting. Cells were lysed with cell lysis buffer (Cell signalling), treated with Benzonase Nuclease (70664 Millipore) and boiled for 5 min. Samples were then run on 4%–12% Bis Tris gels and transferred onto nitrocellulose or PVDF membranes using an iBlot or semidry (Life Technologies and Biorad, respectively).

Membranes were blocked for 1 hour in 5% non-fat milk in PBS + 0.1% Tween-20 (PBST) at room temperature with agitation, incubated in primary antibody (anti-SARS-CoV-2 Spike, which detects the S2 subunit of SARS-CoV-2 S (Invitrogen, PA1-41165), anti-GAPDH (proteintech) or anti-p24 (NIBSC)) diluted in 5% non-fat milk in PBST for 2 hours at 4°C with agitation, washed four times in PBST for 5 minutes at room temperature with agitation and incubated in secondary antibodies anti-rabbit HRP (1:10000, Invitrogen 31462), anti-bactin HRP (1:5000; sc-47778) diluted in 5% non-fat milk in PBST for 1 hour with agitation at room temperature. Membranes were washed four times in PBST for 5 minutes at room temperature and imaged directly using a ChemiDoc MP imaging system (Bio-Rad).

Serum pseudotype neutralisation assay

Spike pseudotype assays have been shown to have similar characteristics as neutralisation testing using fully infectious wild type SARS-CoV-2[39].Virus neutralisation assays were performed on 293T cell transiently transfected with ACE2 and TMPRSS2 using SARS-CoV-2 spike pseudotyped virus expressing luciferase[40]. Pseudotyped virus was incubated with serial dilution of heat inactivated human serum samples or convalescent plasma in duplicate for 1h at 37˚C. Virus and cell only controls were also included. Then, freshly trypsinized 293T ACE2/TMPRSS2 expressing cells were added to each well. Following 48h incubation

in a 5% CO_2 environment at 37°C, the luminescence was measured using Steady-Glo Luciferase assay system (Promega).

Neutralization Assays for convalescent plasma

Convalescent sera from healthcare workers at St. Mary's Hospital at least 21 days since PCR-confirmed SARS-CoV-2 infection were collected in May 2020 as part of the REACT2 study with ethical approval from South Central Berkshire B Research Ethics Committee (REC ref: 20/SC/0206; IRAS 283805).

Convalescent human serum samples were inactivated at 56°C for 30 min and replicate serial 2-fold dilutions (n=12) were mixed with an equal volume of SARs-CoV-2 (100 TCID50; total volume 100 µL) at 37°C for 1 h. Vero-hACE2 TMPRSS2 cells were subsequently infected with serial-fold dilutions of each sample for 3 days at 37°C. Virus neutralisation was quantified via crystal violet staining and scoring for cytopathic effect (CPE). Each-run included 1/5 dilutions of each test sample in the absence of virus to ensure virus-induced CPE in each titration. Back-titrations of SARs-CoV-2 infectivity were performed to demonstrate infection with ~100 TCID50 in each well.

Vaccinee Serum neutralization, live virus

Vero-Ace2-TMPRSS2 cells were seeded at a cell density of 2x10e4/well in 96w plate 24h before infection. Serum was titrated starting at a final 1:10 dilution with WT (SARS-CoV-2/human/Liverpool/REMRQ0001/2020), B1.1.7 or B1.617.2 virus isolates being added at MOI 0.01. The mixture was incubated 1h prior adding to cells. The plates were fixed with 8% PFA 72h post-infection and stained with Coomassie blue for 20 minutes. The plates were washed in water and dried for 2h. 1% SDS was added to wells and staining intensity was measured using FLUOstar Omega (BMG Labtech). Percentage cell survival was determined by comparing intensity of staining to an uninfected wells. A non linear sigmoidal 4PL model (Graphpad Prism 9) was used to determine the ID50 for each serum.

Lung organoid infection by replication competent SARS-CoV-2 isolates.

Airway epithelial organoids were prepared as previously reported. [7] For viral infection primary organoids were passaged and incubated with SARS-CoV-2 in suspension at a multiplicity of infection (MOI) of 1 for 2 hours. Subsequently, the infected organoids were

washed twice with PBS to remove the viral particles. Washed organoids were plated in 20 µl Matrigel domes, cultured in organoid medium and harvested at different timepoints. Cells were lysed 24 and 48h post-infection and total RNA isolated. cDNA was synthesized and qPCR was used to determine copies of nucleoprotein gene in samples. Standard curve was prepared using SARS-CoV-2 Positive Control plasmid containing full nucleocapsid protein (N gene) (NEB) and used to quantify copies of N gene in organoid samples. 18S ribosomal RNA was used as a housekeeping gene to normalize sample-to-sample variation.

Data availability

All fasta consensus sequences files are available for download from https://github.com/Steven-Kemp/hospital_india/tree/main/consensus_fasta

Author contributions

Conceived study: AA, PR, SAK, DC, SB, SF, SM, RKG, DAC. Designed study and experiments: BM, RKG, JB, NG, LCJ, GP, IATM. Performed experiments: IATM, BM, DAC, RD, IATMF, LCG, GBM. Interpreted data: RKG, AA, SS, JB, RP, PC, PD, KP, VSR, SS, DC, TP, OC, GP, LCJ, WB, SF, SB, DAC, BM, RD, IATMF, PR, JB, KGCS. S.M, C.W, T.M, S.B, and S.F. performed mathematical modelling.

Acknowledgments

We would like to thank the Department of Biotechnology, NCDC, RKG is supported by a Wellcome Trust Senior Fellowship in Clinical Science (WT108082AIA). COG-UK is supported by funding from the Medical Research Council (MRC) part of UK Research & Innovation (UKRI), the National Institute of Health Research (NIHR) and Genome Research Limited, operating as the Wellcome Sanger Institute. This study was supported by the Cambridge NIHRB Biomedical Research Centre. We would like to thank Thushan de Silva. SAK is supported by the Bill and Melinda Gates Foundation via PANGEA grant: OPP1175094. I.A.T.M.F. is funded by a SANTHE award (DEL-15-006). We would like to thank Paul Lehner for Calu-3 cells. We thank the Geno2pheno UK consortium. The authors acknowledge support from the G2P-UK National Virology consortium funded by MRC/UKRI (grant ref: MR/W005611/1).This study was also supported by The Rosetrees Trust. SF acknowledges the EPSRC (EP/V002910/1).

References

1 Volz, E. *et al.* Assessing transmissibility of SARS-CoV-2 lineage B.1.1.7 in England. *Nature*, doi:10.1038/s41586-021-03470-x (2021).

2 Collier, D. A. *et al.* SARS-CoV-2 B.1.1.7 sensitivity to mRNA vaccine-elicited, convalescent and monoclonal antibodies. *Nature* **593**, 136-141, doi:10.1101/2021.01.19.21249840 (2021).

3 Cherian, S. *et al.* Convergent evolution of SARS-CoV-2 spike mutations, L452R, E484Q and P681R, in the second wave of COVID-19 in Maharashtra, India. *bioRxiv*, 2021.2004.2022.440932, doi:10.1101/2021.04.22.440932 (2021).

4 Faria, N. R. *et al.* Genomics and epidemiology of the P.1 SARS-CoV-2 lineage in Manaus, Brazil. *Science* **372**, 815-821, doi:10.1126/science.abh2644 (2021).

5 Velumani, A. *et al.* SARS-CoV-2 Seroprevalence in 12 Cities of India from July-December 2020. *medRxiv*, 2021.2003.2019.21253429, doi:10.1101/2021.03.19.21253429 (2021).

6 Rambaut, A. *et al.* A dynamic nomenclature proposal for SARS-CoV-2 lineages to assist genomic epidemiology. *Nat Microbiol* **5**, 1403-1407, doi:10.1038/s41564-020-0770-5 (2020).

7 Youk, J. *et al.* Three-Dimensional Human Alveolar Stem Cell Culture Models Reveal Infection Response to SARS-CoV-2. *Cell Stem Cell* **27**, 905-919 e910, doi:10.1016/j.stem.2020.10.004 (2020).

8 Hoffmann, M. *et al.* SARS-CoV-2 Cell Entry Depends on ACE2 and TMPRSS2 and Is Blocked by a Clinically Proven Protease Inhibitor. *Cell* **181**, 271-280 e278, doi:10.1016/j.cell.2020.02.052 (2020).

9 Peacock, T. P. *et al.* The furin cleavage site in the SARS-CoV-2 spike protein is required for transmission in ferrets. *Nat Microbiol*, doi:10.1038/s41564-021-00908-w (2021).

10 Bhoyar, R. C. *et al.* High throughput detection and genetic epidemiology of SARS-CoV-2 using COVIDSeq next-generation sequencing. *PloS one* **16**, e0247115, doi:10.1371/journal.pone.0247115 (2021).

11 Papa, G. *et al.* Furin cleavage of SARS-CoV-2 Spike promotes but is not essential for infection and cell-cell fusion. *PLoS pathogens* **17**, e1009246, doi:10.1371/journal.ppat.1009246 (2021).

12 Cattin-Ortolá, J. *et al.* Sequences in the cytoplasmic tail of SARS-CoV-2 Spike facilitate expression at the cell surface and syncytia formation. *bioRxiv*, 2020.2010.2012.335562, doi:10.1101/2020.10.12.335562 (2021).

13 Kemp, S. A. *et al.* Recurrent emergence and transmission of a SARS-CoV-2 spike deletion H69/V70. *bioRxiv*, 2020.2012.2014.422555, doi:10.1101/2020.12.14.422555 (2021).

14 Winstone, H. *et al.* The Polybasic Cleavage Site in SARS-CoV-2 Spike Modulates Viral Sensitivity to Type I Interferon and IFITM2. *Journal of virology* **95**, e02422-02420, doi:10.1128/jvi.02422-20 (2021).

15 Kemp, S. *et al.* Recurrent emergence and transmission of a SARS-CoV-2 Spike deletion H69/V70. *bioRxiv*, 2020.2012.2014.422555, doi:10.1101/2020.12.14.422555 (2021).

16 Peacock, T. P. *et al.* The furin cleavage site of SARS-CoV-2 spike protein is a key determinant for transmission due to enhanced replication in airway cells. *bioRxiv* (2020).

17 Kemp, S. A. *et al.* SARS-CoV-2 evolution during treatment of chronic infection. *Nature*, doi:10.1038/s41586-021-03291-y (2021).

18 Meng, B. *et al.* Recurrent emergence of SARS-CoV-2 spike deletion H69/V70 and its role in the variant of concern lineage B.1.1.7. *Cell Reports*, 109292, doi:https://doi.org/10.1016/j.celrep.2021.109292 (2021).

19 Malani, A. *et al.* Seroprevalence of SARS-CoV-2 in slums versus non-slums in Mumbai, India. *Lancet Glob Health* **9**, e110-e111, doi:10.1016/S2214-109X(20)30467-8 (2021).

20 Endo, A., Centre for the Mathematical Modelling of Infectious Diseases, C.-W. G., Abbott, S., Kucharski, A. J. & Funk, S. Estimating the overdispersion in COVID-19 transmission using outbreak sizes outside China. *Wellcome Open Res* **5**, 67, doi:10.12688/wellcomeopenres.15842.3 (2020).

21 Wall, E. C. *et al.* Neutralising antibody activity against SARS-CoV-2 VOCs B.1.617.2 and B.1.351 by BNT162b2 vaccination. *Lancet*, doi:10.1016/S0140-6736(21)01290-3 (2021).

22 Planas, D. *et al.* Reduced sensitivity of infectious SARS-CoV-2 variant B.1.617.2 to monoclonal antibodies and sera from convalescent and vaccinated individuals. *bioRxiv*, 2021.2005.2026.445838, doi:10.1101/2021.05.26.445838 (2021).

23 Motozono, C. *et al.* An emerging SARS-CoV-2 mutant evading cellular immunity and increasing viral infectivity. *bioRxiv*, 2021.2004.2002.438288, doi:10.1101/2021.04.02.438288 (2021).

24 Johnson, B. A. *et al.* Loss of furin cleavage site attenuates SARS-CoV-2 pathogenesis. *Nature* **591**, 293-299, doi:10.1038/s41586-021-03237-4 (2021).

25 Braga, L. *et al.* Drugs that inhibit TMEM16 proteins block SARS-CoV-2 Spike-induced syncytia. *Nature*, doi:10.1038/s41586-021-03491-6 (2021).

26 Shinde, V. *et al.* Efficacy of NVX-CoV2373 Covid-19 Vaccine against the B.1.351 Variant. *New England Journal of Medicine*, doi:10.1056/NEJMoa2103055 (2021).

27 Abu-Raddad, L. J., Chemaitelly, H. & Butt, A. A. Effectiveness of the BNT162b2 Covid-19 Vaccine against the B.1.1.7 and B.1.351 Variants. *New England Journal of Medicine*, doi:10.1056/NEJMc2104974 (2021).

28 Madhi, S. A. *et al.* Efficacy of the ChAdOx1 nCoV-19 Covid-19 Vaccine against the B.1.351 Variant. *N Engl J Med*, doi:10.1056/NEJMoa2102214 (2021).

29 Sadoff, J. *et al.* Safety and Efficacy of Single-Dose Ad26.COV2.S Vaccine against Covid-19. *New England Journal of Medicine*, doi:10.1056/NEJMoa2101544 (2021).

30 Katoh, K. & Standley, D. M. MAFFT multiple sequence alignment software version 7: improvements in performance and usability. *Mol Biol Evol* **30**, 772-780, doi:10.1093/molbev/mst010 (2013).

31 Minh, B. Q. *et al.* IQ-TREE 2: New models and efficient methods for phylogenetic inference in the genomic era. *bioRxiv*, 849372, doi:10.1101/849372 (2019).

32 Yu, G., Smith, D. K., Zhu, H., Guan, Y. & Lam, T. T. Y. ggtree: an R package for visualization and annotation of phylogenetic trees with their covariates and other associated data. *Methods in Ecology and Evolution* **8**, 28-36 (2017).

33 Shu, Y. & McCauley, J. GISAID: Global initiative on sharing all influenza data - from vision to reality. *Euro surveillance : bulletin Europeen sur les maladies transmissibles = European communicable disease bulletin* **22**, 30494, doi:10.2807/1560-7917.ES.2017.22.13.30494 (2017).

34 Wrobel, A. G. *et al.* SARS-CoV-2 and bat RaTG13 spike glycoprotein structures inform on virus evolution and furin-cleavage effects. *Nat Struct Mol Biol* **27**, 763-767, doi:10.1038/s41594-020-0468-7 (2020).

35 Vermeire, J. *et al.* Quantification of reverse transcriptase activity by real-time PCR as a fast and accurate method for titration of HIV, lenti- and retroviral vectors. *PloS one* **7**, e50859-e50859, doi:10.1371/journal.pone.0050859 (2012).

36 Kodaka, M. *et al.* A new cell-based assay to evaluate myogenesis in mouse myoblast C2C12 cells. *Experimental cell research* **336**, 171-181 (2015).

37 Papa, G. *et al.* Furin cleavage of SARS-CoV-2 Spike promotes but is not essential for infection and cell-cell fusion. *PLoS Pathogens* **17**, e1009246 (2021).

38 Buchrieser, J. *et al.* Syncytia formation by SARS-CoV-2-infected cells. *The EMBO journal* **39**, e106267 (2020).

39 Schmidt, F. *et al.* Measuring SARS-CoV-2 neutralizing antibody activity using pseudotyped and chimeric viruses. 2020.2006.2008.140871, doi:10.1101/2020.06.08.140871 %J bioRxiv (2020).

40 Mlcochova, P. *et al.* Combined point of care nucleic acid and antibody testing for SARS-CoV-2 following emergence of D614G Spike Variant. *Cell Rep Med*, 100099, doi:10.1016/j.xcrm.2020.100099 (2020).

INSACOG CONSORTIUM MEMBERS

NIBMG: Saumitra Das, Arindam Maitra, Sreedhar Chinnaswamy, Nidhan Kumar Biswas;

ILS: Ajay Parida, Sunil K Raghav, Punit Prasad;

InSTEM/ NCBS: Apurva Sarin, Satyajit Mayor, Uma Ramakrishnan, Dasaradhi Palakodeti, Aswin Sai Narain Seshasayee;

CDFD: K Thangaraj, Murali Dharan Bashyam, Ashwin Dalal;

NCCS: Manoj Bhat, Yogesh Shouche, Ajay Pillai;

IGIB: Anurag Agarwal, Sridhar Sivasubbu, Vinod Scaria;

NIV: Priya Abraham, Potdar Varsha Atul, Sarah S Cherian;

NIMHANS: Anita Sudhir Desai, Chitra Pattabiraman, M. V. Manjunatha, Reeta S Mani, Gautam Arunachal Udupi;

NCDC: Sujeet Singh, Himanshu Chauhan, Partha Rakshit, Tanzin Dikid;

CCMB: Vinay Nandicoori, Karthik Bharadwaj Tallapaka, Divya Tej Sowpati

INSACOG collaborating divisions and clinical partners

Biotechnology division, NCDC: Hema Gogia, Hemlata Lall, Kalaiarasan Ponnusamy, Kaptan Verma, Mahesh S Dhar, Manoj K Singh, Meena Datta, Namita Soni, Namonarayan Meena, Partha Rakshit, Preeti Madan, Priyanka Singh, Radhakrishnan V. S, Ramesh Sharma, Rajeev Sharma, Robin Marwal, Sandhya Kabra, Sattender Kumar, Swati Kumari, Uma Sharma, Urmila Chaudhary
Integrated Disease Surveillance Program (IDSP), NCDC, Central and State IDSP units

Centre of Epidemiology, NCDC

Sir Ganga Ram Hospital, Rajinder Nagar, New Delhi: Dept of Clinical Microbiology & Immunology and Director Medical Hospital Administration, Chand Wattal, J K Oberoi, Neeraj Goel, Reena Raveendran, S. Datta

Northern Railway Central Hospital, Basant Lane, New Delhi: Meenakshi Agarwal

Indraprastha Apollo Hospitals, New Delhi: Administration and Microbiology department, Raju Vaishya

1
2
3
4

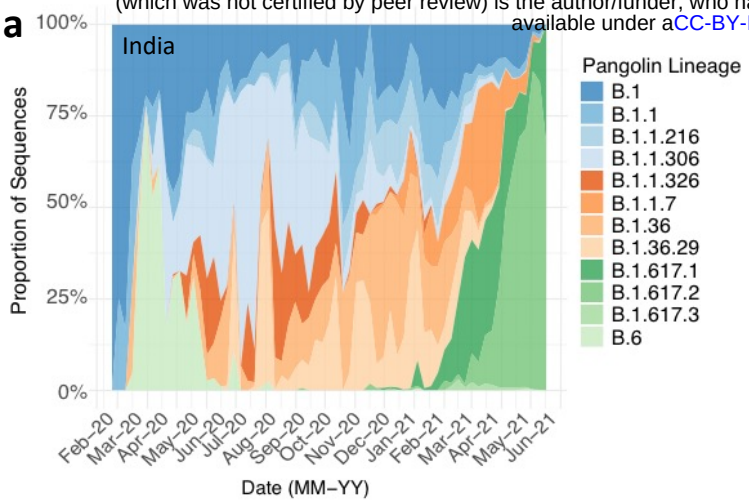

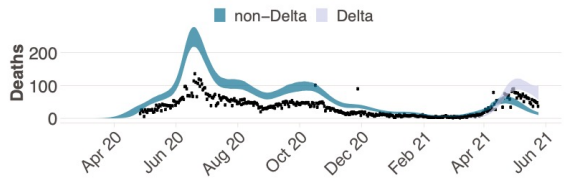

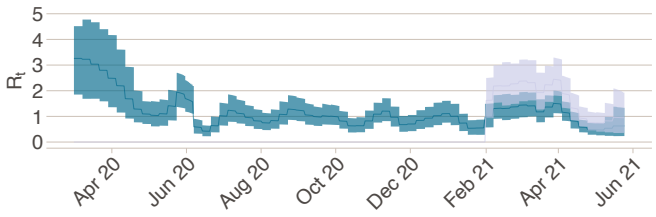

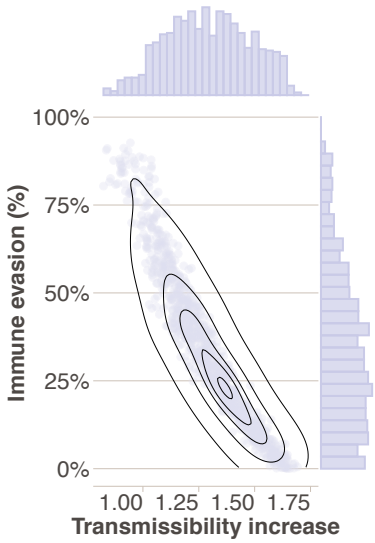

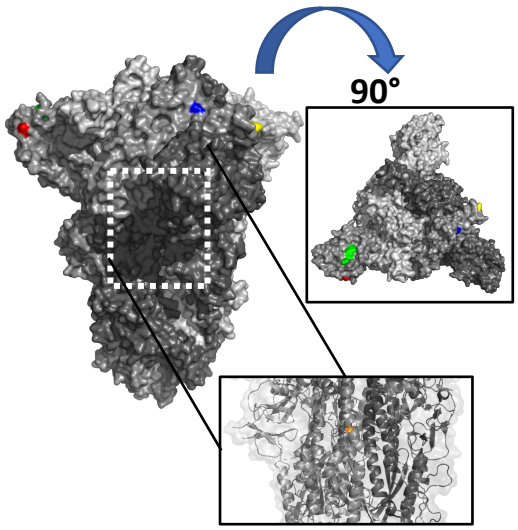

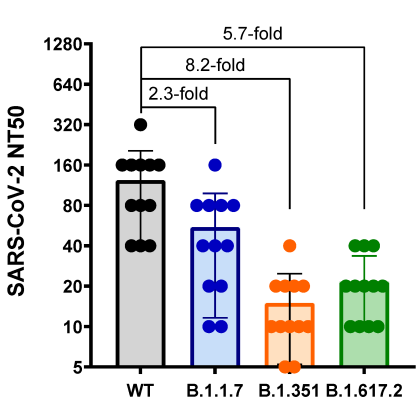

Figure. 1. **Rapid Expansion of Delta variant B.1.617.2 in India with immune evasion and increased transmissibility a.** Proportion of lineages in incident cases of SARS-CoV-2 in India 2020-2021. **b-d**. Modelling resurgence of SARS-CoV-2 transmission in Mumbai and the epidemiological characteristics of delta variant B.1.617.2, inferred using a two category Bayesian transmission model[1] fitted to COVID-19 mortality, serological and genomic sequence data. The introduction date for B.1.671.2 is set to 31st Jan 2021 and 50% under-reporting in COVID-19 mortality data is assumed. **b.** Daily incidence of COVID-19 mortality with black dots showing the observed data. Coloured lines show the mean of posterior estimates of true number of deaths (i.e. after accounting for 50% underreporting) and shaded region representing the 95% CI, with the blue line showing deaths attributed to non-delta variant lineages and the orange line showing deaths attributed to delta variant. **c.** Bayesian posterior estimates of trends in the reproduction number (R_t) for the delta and non-delta variant categories**. d.** Joint posterior distribution of the inferred transmissibility increase and degree of immune evasion (predominantly re-infection in India due to low vaccination coverage) for delta (relative to non-delta variant categories). Grey contours refer to posterior density intervals ranging from the 95% and 5% isoclines. Marginal posterior distributions for each parameter shown along each axis. **e.** Surface representation of the SARS-CoV-2 Delta variant Spike trimer (PDB: 6ZGE). L19R (red), del157/158 (green) L452R (blue) and T478K (yellow). The white dashed box indicates the location of the D950N (orange) **f. Neutralization of Delta variant by convalescent human serum from mid-2020** in Vero-hACE2 TMPRSS2 cells. Fold-change in serum neutralization 100 $TCID_{50}$ of B.1.17 (Alpha-UK), B.1.351 (Beta- South Africa) and B.1617 (Delta-India) variants relative to wild-type (IC19), n=12.

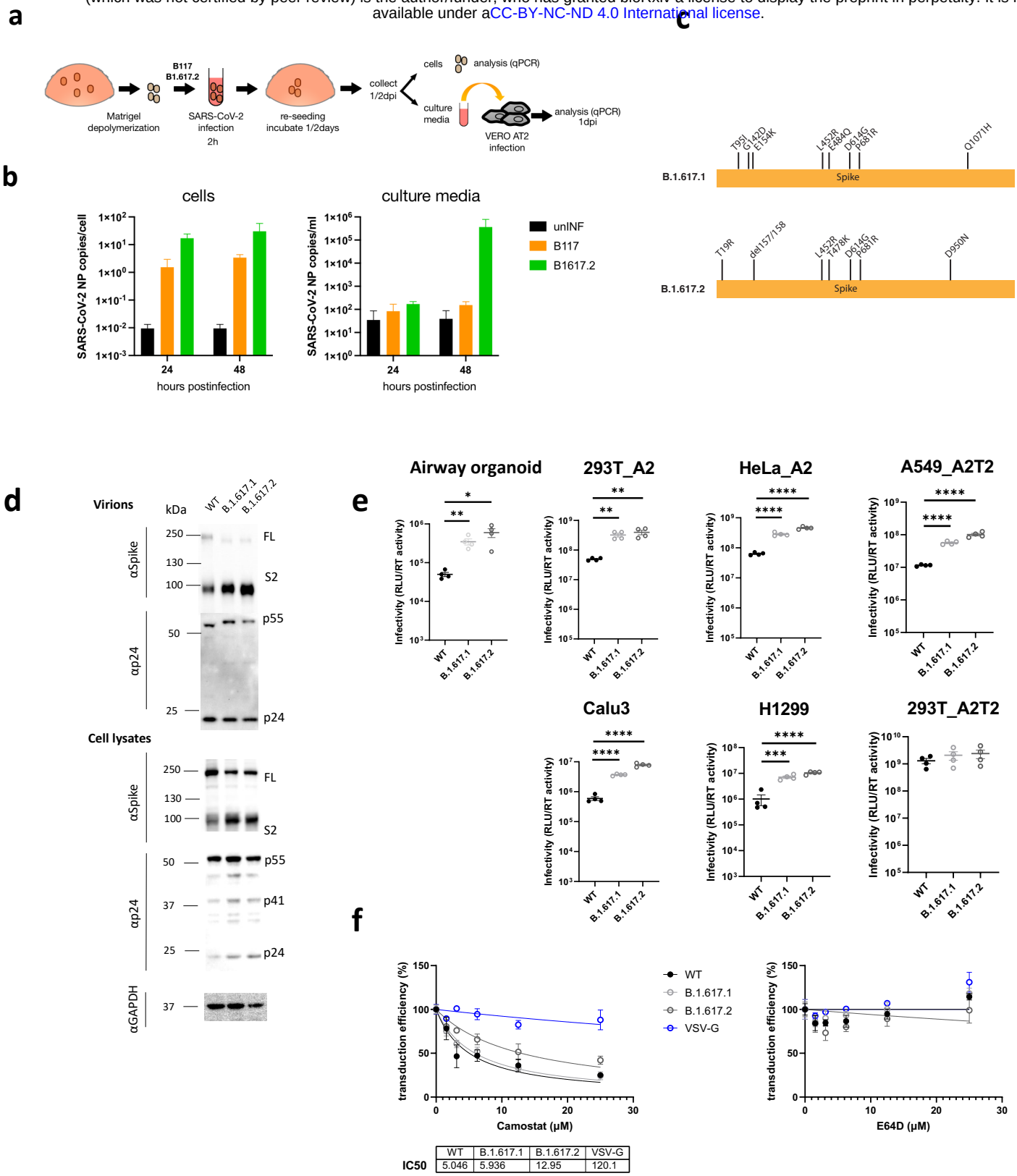

Figure 2. a. **SARS-CoV-2 Delta Variant replication and and spike mediated entry efficiency. a,b. Live virus r**eplication in airway epithelial organoid cultures. **a.** Airway epithelial organoids were infected with SARS-CoV-2 Alpha and Delta variants at MOI 1. Cells were lysed 24 and 48h post-infection and total RNA isolated. **b.** qPCR was used to determine copies of nucleoprotein gene in organoid cells and infectivity of cell free virus measured by infection of Vero AT2 cells). Data represent the average of two independent experiments. **B.1.617.2 delta variant spike confers increased cell entry and is accompanied by increased incorporation of cleaved spike into virions. C.** diagram showing mutations present in spike plasmids used **d.** Western blots of pseudotyped virus (PV) virions and cell lysates of 293T producer cells following transfection with plasmids expressing lentiviral vectors and SARS-CoV-2 S B.1.617.1 and Delta variant B.1.617.2 versus WT (all with D614G), probed with antibodies for HIV-1 p24 and SARS-Cov-2 S2. **e.** Single round infectivity on different cell targets by spike B1.617 versus WT PV produced in 293T cells. Data are representative of three independent experiments. **f**. PV Infection of A549 cells stably expressing ACE2 and TMPRSS2 in the presence of increasing doses of the TMPRSS2 inhibitor camostat or the cathepsin inhibitor E64D. IC50 values are shown. Data are shown with mean and standard error of mean (SEM) and the statistics were performed using unpaired Student t test.

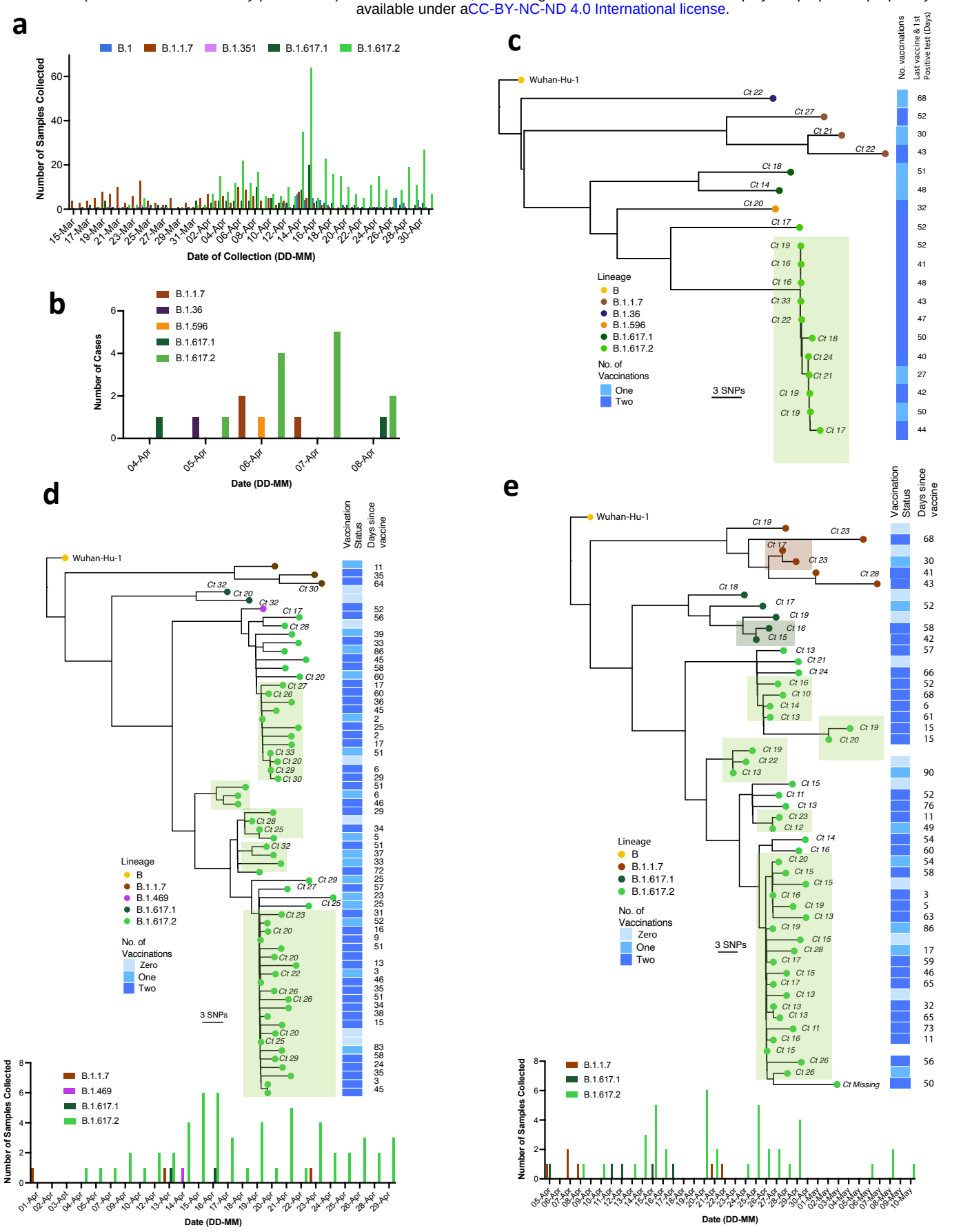

Figure 3. SARS-CoV-2 B.1.617.2 infection and transmission clusters in vaccinated HCW at three Delhi health care centres. a. Case frequencies of five most commonly occurring SARS CoV-2 lineages over time for a. Delhi and **b**. for a single health care centre amongst vaccinated HCW. **b-d** Maximum likelihood phylogenies of vaccine breakthrough SARS-CoV-2 sequences amongst vaccinated HCW at three centres are presented. Phylogenies were inferred with IQTREE2 with 1000 bootstrap replicates. Trees are rooted on Wuhan-Hu-1 and annotated with the lineage designated by pangolin v.2.4.2. The number of COVISHIELD (ChAdOx-1) vaccinations received by each individual is indicated by the heatmap to the right. White space indicates missing data. The number indicated is the time, in days, between the last vaccination and the sample collection. At the bottom of each tree is a case frequency graph by date of testing. Shaded areas, coloured according to lineage, show inferred transmission clusters of 2 or more sequences

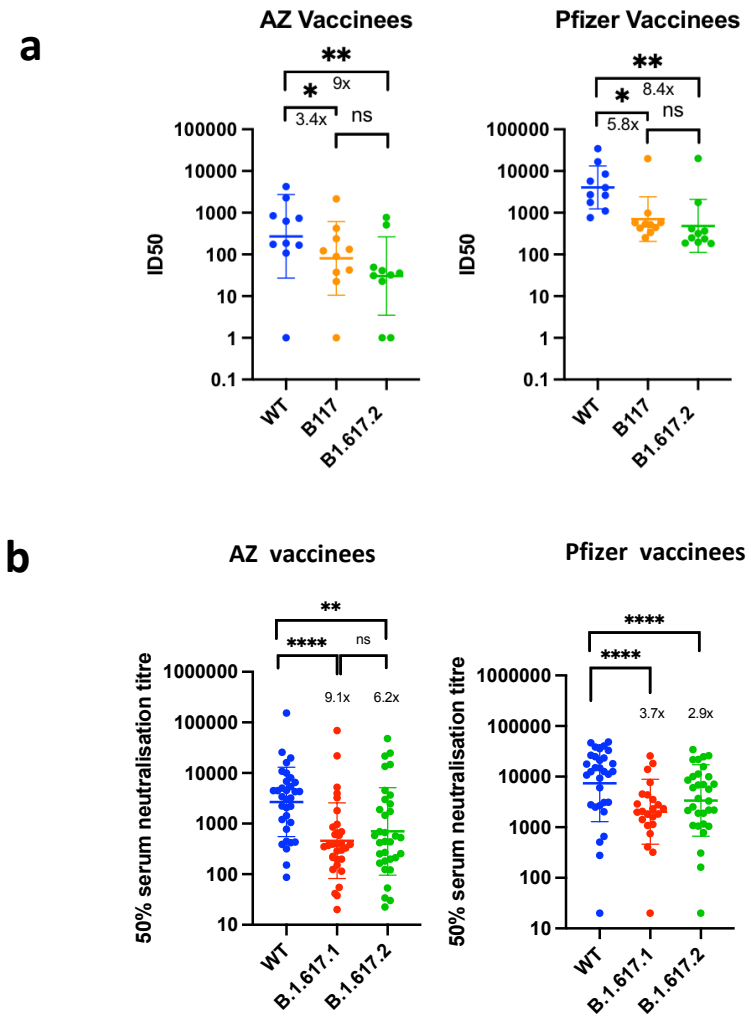

Figure 4: Delta variant B.1.617.2 shows reduced sensitivity to neutralizing antibodies from sera derived following vaccination. a. Neutralisation of delta variant live virus isolate by sera from vaccinated individuals (n=10 ChAdOx-1 or n=10 BNT12b2) in comparison to B.1.1.7 Alpha variant and Wuhan-1 wild type. **5**-fold dilutions of vaccinee sera were mixed with wild type (WT) or viral variants (MOI 0.1) for 1h at 37˚C. Mixture was added to Vero-hACE2/TMPRSS2 cells for 72h. Cells were fixed and stained with Coomasie blue and % of survival calculated. ID50 were calculated using nonlinear regression. Graph represents average of two independent experiments.**b.** Neutralisation of B.1.617 spike pseudotyped virus (PV) and wild type (D614G background) by vaccine sera (n=33 ChAdOx-1 or n=32 BNT12b2). GMT (geometric mean titre) with s.d are presented. Data representative of two independent experiments each with two technical repeats. **p<0.01, *** p<0.001, ****p<0.0001 Wilcoxon matched-pairs signed rank test, ns not significant.

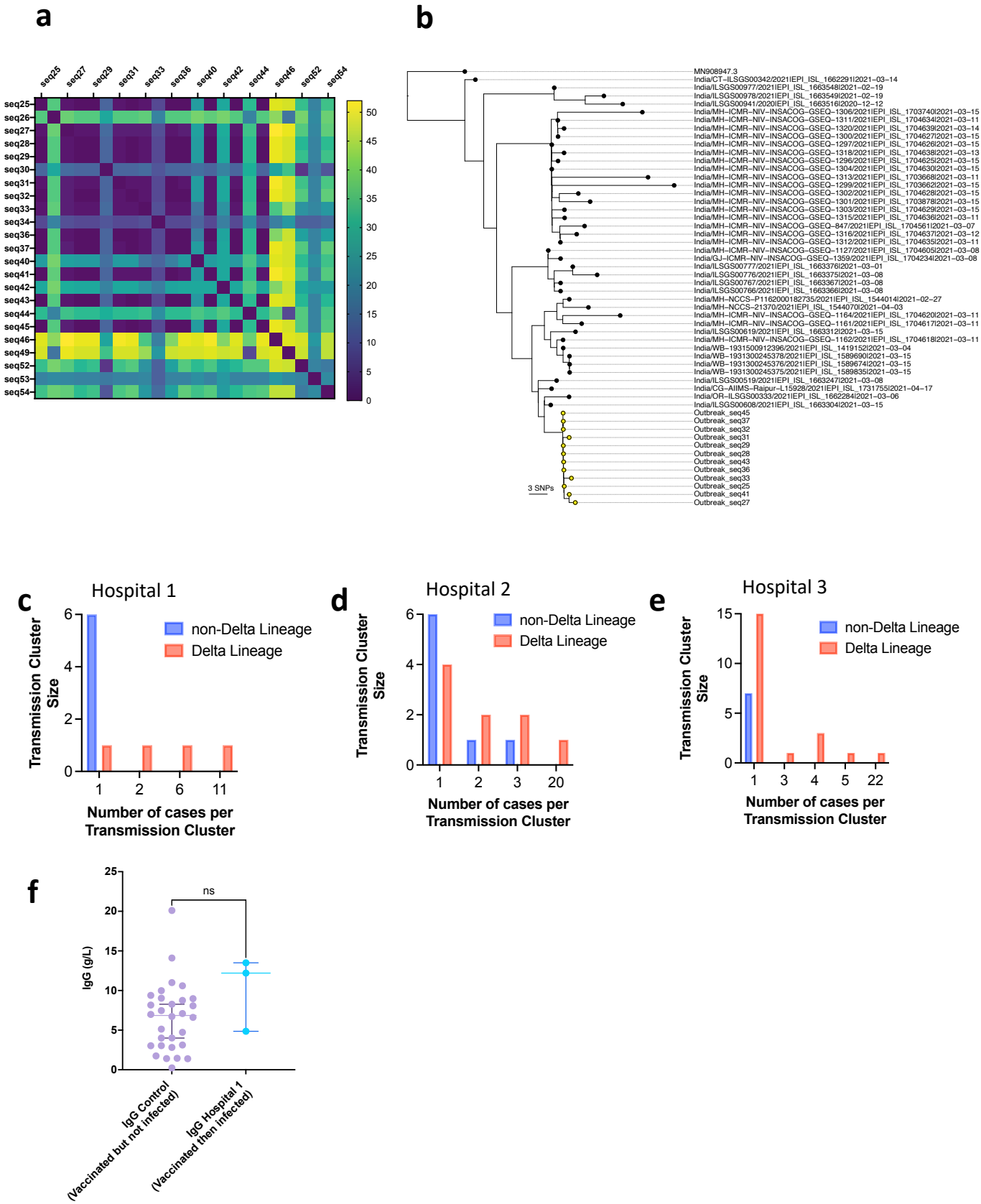

Extended Data Figure 1. Breakthrough SARS-CoV-2 infections amongst vaccinated health care workers (HCW) a. A heatmap of pairwise SARS-CoV-2 SNP differences of vaccinated HCW samples at hospital 1**.** The B.1.617.2 lineage is in the upper-left quarter, with fewer than 2 SNP difference between them. **b.** Maximum likelihood phylogeny of vaccine breakthrough SARS-CoV-2 B.1.617.2 sequences from hospital 1 in context of closest Indian B.1.617.2 sequences. Phylogeny was inferred with IQTREE2 with 1000 bootstrap replicates. Rooted on Wuhan-Hu-1 and annotated with the lineage designated by pangolin v.3.0.5. **c-e**. Frequency graphs for cluster size at each hospital 1-3. **f**. Comparison of IgG antibody titres between a control group of vaccinated individuals receiving two doses of ChadOx-1 who have not been infected with SARS-CoV-2, with vaccinated healthcare workers who had received two doses and subsequently tested positive for SARS-CoV-2.

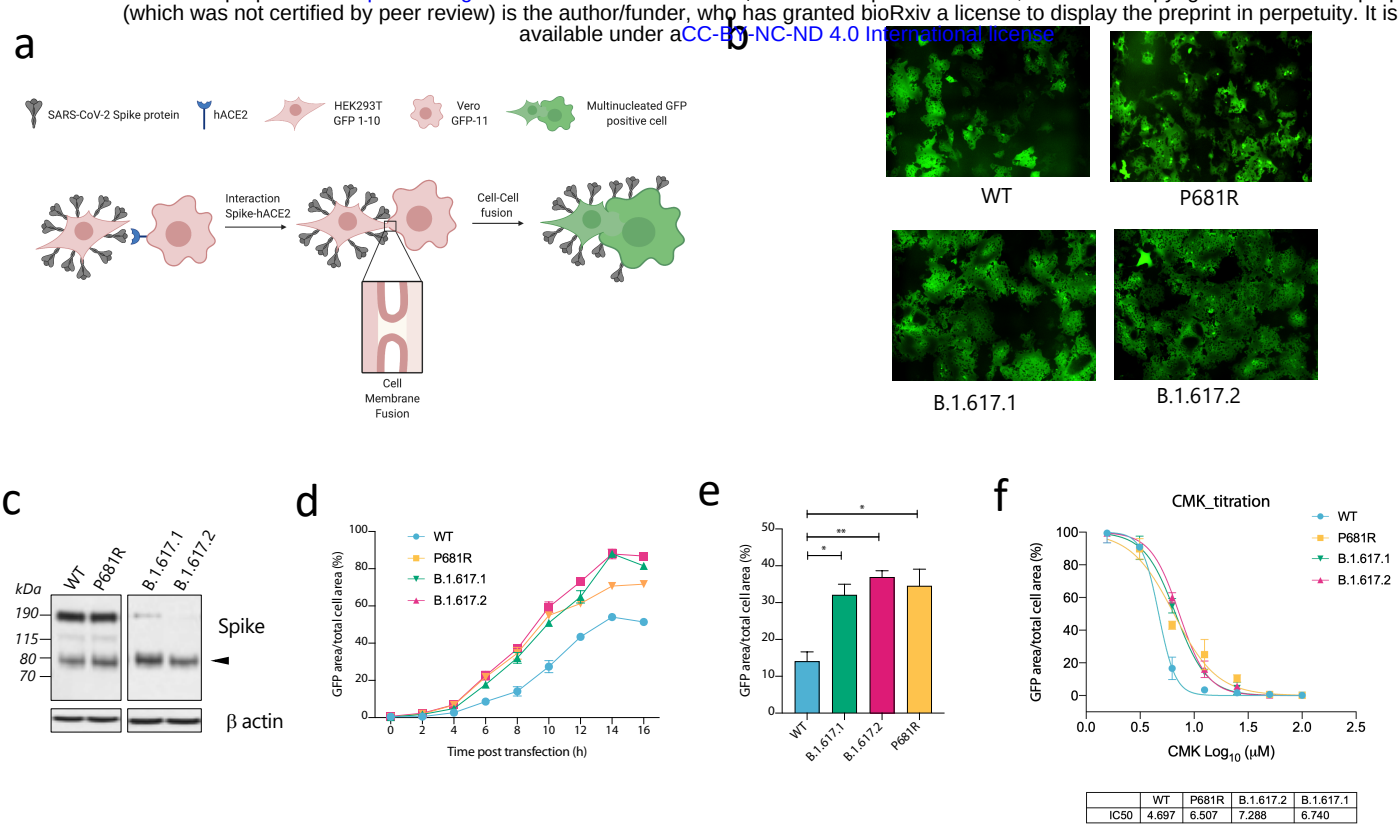

	WT	P681R	B.1.617.2	B.1.617.1
IC50	4.697	6.507	7.288	6.740

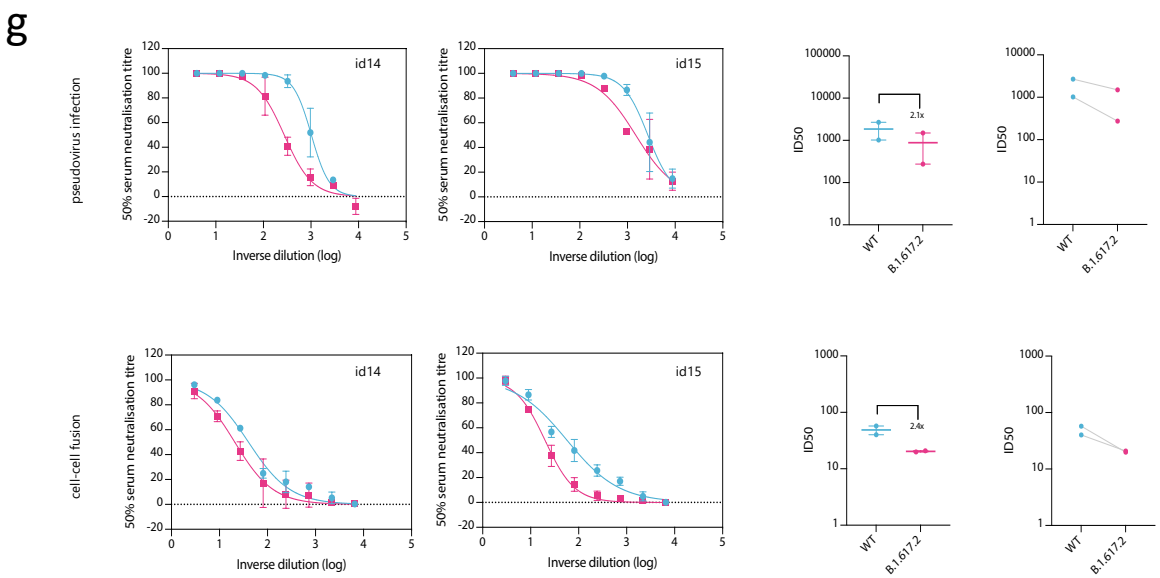

Extended Data Figure 2: B.1.617.2 Delta variant spike confers accelerated cell-cell fusion activity that can be blocked by anti-spike neutralising antibodies in sera. a. Schematic of cell-cell fusion assay. **b.** Reconstructed images at 10 hours of GFP positive syncytia formation. Scale bars represent 400 mm. c. western blot of cell lysates 48 hours after transfection of spike plasmids. Anti-S2 antibody. **d,e.** Quantification of cell-cell fusion kinetics showing percentage of green area to total cell area over time. Mean is plotted with error bars representing SEM**. f**. Sensitivity of fusion kinetics to furin inhibitor CMK as shown by titration of drug and measurement of fusion after 10hrs. Mean is plotted with error bars representing SEM. **g**. comparison of impact of post vaccine sera (n=2) on PV neutralisation (top) and cell-cell fusion (bottom), comparing WT and Delta variant B.1.671.2.